THE ASTROPHYSICAL JOURNAL, 405:464–478, 1993 March 10

SATELLITES OF SPIRAL GALAXIES[1]

DENNIS ZARITSKY,[2,3] RODNEY SMITH,[4] CARLOS FRENK,[5,6] AND SIMON D. M. WHITE[2,7]

Received 1992 April 20; accepted 1992 September 15

ABSTRACT

We present a survey of satellites around a homogeneous set of late-type spirals with luminosity similar to that of the Milky Way. The survey aims to probe the mass distribution at galactocentric radii ~ 250 kpc. The 69 satellites in our sample span a range of magnitudes similar to that of the brighter satellites in the Local Group. Slightly over half the objects are new discoveries. Existing data were supplemented by our observations of radial velocities to obtain km s^{-1} precision. In this paper we present the data and carry out a first-cut dynamical analysis. On average, we find fewer than 1.5 satellites per primary, but we argue that we can treat the survey as an *ensemble* and so derive the properties of the halo of a "typical" isolated spiral. The projected density profile of the ensemble falls off approximately as r^{-1}. Within 50 kpc the azimuthal distribution of satellites shows some evidence for the "Holmberg effect," an excess near the minor axis of the primary; however, at larger projected distances, the distribution appears isotropic. There is a weak but significant correlation between the size of a satellite and its distance from its primary, as expected if satellites are tidally truncated. Neither Hubble type nor spectral characteristics correlate with apparent separation. The ensemble of satellites appears to be rotating at about 30 km s^{-1} in the same direction as the galactic disk. Satellites on prograde orbits tend to be brighter than those on retrograde orbits. The typical velocity difference between a satellite and its primary shows no clear dependence either on apparent separation, or on the rotation speed of the primary. Naive mass estimates suggest that the mass contained within 200 kpc is of order $2 \times 10^{12}\ M_\odot$. Thus our survey demonstrates that isolated spiral galaxies have massive halos that extend to many optical radii.

Subject headings: galaxies: clustering — galaxies: distances and redshifts — galaxies: fundamental parameters — galaxies: spiral

1. INTRODUCTION

In the 1970s, the discovery of massive halos around spiral galaxies revolutionized the study of galactic structure and provided one of the cornerstones of our present understanding of galaxy formation (Rubin & Ford 1970; Freeman 1970; White & Rees 1978). It is commonly believed that the dark halos of typical galaxies extend far beyond their optical radius and have a mass of at least $10^{12}\ M_\odot$. Indeed, such halos are a generic prediction of hierarchical clustering theories for galaxy formation, which suggest that in a flat universe the halo of a bright galaxy will extend out until it meets that of its neighbor. However, much of this theoretical prejudice is singularly lacking in observational support. Until now the best evidence for dark matter around spirals has come from H I rotation curves. At best, these can be measured out to only a few optical radii (e.g., Begeman 1987).

The conventional notion that dark halos are very extended was tested by Little & Tremaine (1987). In an elegant paper, they argued that the small radial velocity dispersion of the 10 distant satellites of the Milky Way with "good" data required the Galactic halo to terminate at $r \lesssim 50$ kpc, and to have a mass, $M \simeq 2.5 \times 10^{11}\ M_\odot$. At about the same time, Erickson, Gottesman, & Hunter (1987) studied the kinematics of small groups of satellites around nine spiral galaxies and claimed that these data were also consistent with small dark halos. Although satellite galaxies probe regions beyond those reached by H I rotation curves, these particular studies were dominated by nearby satellites and were also limited by the small number of satellites detected around each individual galaxy; the most populous system in the sample of Erickson et al. had only five satellites. Even with the 10 Galactic satellites considered by Little & Tremaine, large uncertainties remained. By 1991 accurate velocities were available for a further six objects, and the mass estimate from the Little-Tremaine estimator had increased by a factor of 5 to $M \simeq 12.5 \times 10^{11}\ M_\odot$ (Zaritsky et al. 1989; Zaritsky 1991). More than half of this change is due to a single system Leo I, which is both distant (230 kpc) and rapidly moving (180 km s^{-1}). With supporting evidence from Local Group timing arguments (cf. Einasto & Lynden-Bell 1982; Zaritsky et al. 1989) and the analysis of halo star samples that are beginning to become available (Norris & Hawkins 1991), the data for our own Galaxy seem once more to indicate the presence of an extended massive halo.

In a classic paper, Holmberg (1969) demonstrated that satellites are quite rare. He used the Palomar Observatory Sky Survey (POSS) plates to count faint images around bright galaxies. After correcting for background contamination through counts at a much larger projected distance, he concluded that spirals have between one and five satellites within ~ 50 kpc to an absolute magnitude limit which he estimated to be -10.6.

[1] This work is based in part on observations carried out at the Multiple Mirror Telescope Observatory, a joint facility of the University of Arizona and the Smithsonian Institution, and at the Cerro Tololo Inter-American Observatory, operated by the Association of Universities for Research in Astronomy, Inc., under contract with the National Science Foundation.

[2] Steward Observatory, University of Arizona, Tucson, AZ 85721.

[3] Hubble Fellow. Presently at The Observatories of the Carnegie Institution of Washington, 813 Santa Barbara Street, Pasadena, CA 91101.

[4] Department of Physics, P.O. Box 913, University of Wales, College of Cardiff, Cardiff CF1 3TH, Wales.

[5] Department of Physics, South Road, University of Durham, Durham DH1 3LE, England.

[6] Nuffield Foundation Science Research Fellow.

[7] Institute of Astronomy, Madingley Road, University of Cambridge, CB3 0HA, England.

In this study he also discovered the "Holmberg effect," an apparent excess of satellites along the minor axis of nearly edge-on spirals. More recently, Lorrimer et al. (1993) have repeated Holmberg's survey using digitized scans of POSS and ESO/SERC (UK Schmidt) Sky Survey plates. They find that the typical late-type galaxy has only about one satellite brighter than $M_B = -16.5$ within 375 kpc.[8]

The approach we follow in this paper to overcome the severe limitation imposed by small satellite numbers is through the statistical treatment of satellites around a large sample of parent galaxies. Its underlying philosophy is that the satellites of a suitably defined sample of galaxies can be treated as an *ensemble*. Clearly, the results will be difficult to interpret unless selection of the sample of primary galaxies ensures that their dynamical properties are similar. The well-known correlations between disk circular velocity, luminosity, and Hubble type (Tully & Fisher 1977; Rubin, Ford, & Thonnard 1978; Rubin, Burstein, & Thonnard 1980), suggest that selection of a homogeneous sample is a reasonable goal. However, one must bear in mind that while we select galaxies according to optical criteria, the regions that interest us lie well outside their visible components.

A few years ago we embarked on a program to identify a large sample of satellites around isolated spiral galaxies and to measure their radial velocities using multiobject spectroscopy. Our aim was to study the mass and extent of dark halos around galaxies like the Milky Way. The original program envisaged the dual use of the MX multifiber system at the Steward Observatory 2.3 m telescope and the AUTOFIB fiber systems at the Anglo-Australian and William Herschel telescopes (the AAT and WHT, respectively). However, unusually bad weather at the UK sites resulted in almost all the work being done on the University of Arizona and CTIO telescopes. Fortunately, we found that a substantial number of satellites satisfying our selection criteria already had published radial velocities. In this paper, we present data for the sample we have accumulated so far. These are already sufficient to carry out a first analysis, although we plan to enlarge the sample in future. This paper presents a general discussion of the properties of the satellites, together with a first-cut discussion of their ensemble dynamics. A more refined and robust dynamical analysis will be published in two separate papers (White & Zaritsky 1992; Zaritsky & White 1993). A detailed discussion of contamination and projection effects in the sample is given by Zaritsky (1992), while a study of the abundance and radial distribution of satellite galaxies in general is presented by Lorrimer et al. (1993). An independent study of the satellite populations of early type galaxies has recently been published by Vader & Sandage (1991).

The goals and basic approach of our program are reminiscent of studies of binary galaxies (White et al. 1983; Schweizer 1987; Charlton & Salpeter 1991). The major difference is that whereas the members of a typical binary have comparable luminosity, we only consider satellites that are much fainter than their primary. Thus our problem is simpler in many respects. Provided primaries are chosen to have no nearby bright companions, their gravitational potential should be approximately static, and the satellites may be regarded as test particles. We do not, therefore, need to concern ourselves with the dynamical complications that may arise if the halos of two bright galaxies overlap. However, other problems, such as difficulties in identifying and excluding interlopers, are common to both kinds of study.

The remainder of this paper is organized as follows. In § 2 we describe the selection criteria for our sample; in § 3 we describe our multifiber and follow-up observations; in § 4 we present our data, discuss various properties of the sample, and obtain a crude estimate of the mass of the parent galaxies; in § 5 we summarize our results. Our main conclusion is that isolated bright spirals do indeed have very massive extended halos.

2. THE SAMPLE

2.1. *The Selection of Primary Galaxies*

We have already emphasized the importance for our analysis of selecting a homogeneous sample of isolated primary galaxies. We adopted the following selection criteria: (1) A narrow range in absolute magnitude, M_B; (2) Hubble type Sb to Sc, unbarred; (3) recession velocity in the range 1000 km $s^{-1} < v_R < 7000$ km s^{-1}; and (4) isolation.

Because of the well-known correlation between M_B and rotational velocity in spirals (Tully & Fisher 1977), a narrow range in absolute magnitude seems a reasonable requirement for a dynamically homogeneous sample. Nevertheless, for binary galaxies there appears to be only a weak correlation between the velocity difference among a pair and the total luminosity (White et al. 1983). Sixty-three percent of our sample lies in the range $-20.5 < M_B < -19.5$, and 77% in the sightly less restricted range $-21 < M_B < -19$. To test for systematic variations in dynamical properties with primary luminosity, we have also included a small proportion of galaxies in the wider range $-22 < M_B < -18$.

The second criterion was imposed because there is evidence that the morphology of a galaxy determines the form of its rotation curve at least in the inner regions (Rubin et al. 1978). While it is most likely that the presence of a bar is unrelated to the large-scale distribution of dark matter, we nevertheless reject barred galaxies to be conservative. Since there seem to be substantial discrepancies in the classification of barred galaxies in the literature, we inspected all our primaries on POSS or ESO/SERC plates and applied our own classification, rejecting ambiguous cases.

The window in recession velocity was imposed primarily in order to match the field of view of our telescopes (40′–50′) to the physical size of the region of interest around each spiral (a few hundred kiloparsecs). Furthermore, at a distance of 7000 km s^{-1}, an apparent magnitude of 18.5 corresponds to an absolute magnitude of -16.4, only about 2 mag fainter than our faintest primaries. Thus, we cannot go beyond this limit and still detect satellites that are significantly fainter than their parent galaxies. In fact, most of our primaries have recession velocities between 2000 and 4000 km s^{-1} and only a few (those observed at the WHT, which has a field of view of only $\sim 17'$) have $v_R > 5000$ km s^{-1}. The lower cutoff in v_R ensures that the redshift distances of the galaxies are not severely affected by peculiar velocities.

The isolation criterion is rather more complicated. Our primaries must be relatively isolated so that the kinematics of the satellites are undisturbed by tidal fields. To justify our choice of parameters, we argue as follows. In the absence of clustering, the mean separation of galaxies brighter than $M_B = -18$ would be 4.4 Mpc, as may be verified by integrating the Schechter luminosity function with the parameters given by

[8] Throughout this paper we take the Hubble constant to be $H_0 = 75$ km s^{-1} Mpc^{-1}.

Efstathiou et al. (1988a). On the other hand, the mean separation of galaxies in groups is ~ 1.5 Mpc (cf. Nolthenius & White 1987). We therefore expect the nearest bright neighbor to be 1–2 Mpc from a typical candidate primary. With this in mind, we required that all galaxies with a velocity difference, $|\Delta v| < 1000$ km s^{-1}, relative to the primary should satisfy the following conditions:

1. If projected within 500 kpc of the primary, they should be at least 2.2 magnitudes (a factor of 8) fainter.
2. If projected within 1 Mpc of the primary, they should be at least 0.7 magnitudes (a factor of 2) fainter.

We can gauge how stringent these isolation criteria are by considering the Local Group. The two dominant galaxies, the Milky Way and M31, are separated by 0.7 Mpc and have a magnitude difference of 0.6 mag (van den Bergh 1980). Thus, the Local Group would not satisfy our criteria even at the most favorable viewing angle. Yet, at least to a distance of 200 kpc from each galaxy, the dynamics appear to be dominated by the nearer object (cf. Zaritsky et al. 1989; Moore & Frenk 1990). A rough estimate of the likely effect of companions on the dynamics of our satellites may be obtained from the three-body system considered by Schweizer (1987). Suppose the mass of the primary is measured from the motion of a satellite at a distance of 200 kpc. The fractional errors induced in the determination by neglecting a galaxy as massive as the primary and 1 Mpc away, or a galaxy half as massive and 0.5 Mpc away, are of order 0.02 and 0.1, respectively. According to this measure, our isolation criteria are quite conservative.

Our sample of primaries was drawn almost entirely from *z*-cat (Huchra 1987). Having selected a list of candidates satisfying criteria (1) to (3) above, we searched both *z*-cat and the Huchtmeier-Richter (1989) catalog (hereafter HR) for bright companions. The galaxies that passed this preliminary screening were then inspected visually on POSS or ESO/SERC plates for nearby companions that might not appear in the redshift catalogs. At the same time we checked the primaries for bars and dubious cases were excluded. A few of the fields that passed these tests had rich clusters nearby and we also excluded them. We ended up with a sample of nearly 100 primaries. While this is not a complete list, it probably includes the majority of galaxies that satisfy all our criteria.

2.2. *The Search for Satellites*

We define a satellite galaxy as one which (1) lies within a projected separation, $r_p < 500$ kpc, of the primary; (2) is at least 2.2 mag fainter than the primary; and (3) has a velocity difference, $|\Delta v| < 500$ km s^{-1} relative to the primary. We do not impose any morphological restrictions. All these values represent compromises. The first condition reflects our expectation that undisturbed companions will lie well within ~ 2 Mpc of each primary, as discussed above. The second attempts to strike a balance between having genuinely faint satellites and having a sufficiently large number of objects above our observational detection limit, $m_B \sim 18.5$. The last condition is a compromise between eliminating real companions if $|\Delta v|$ is chosen too small, and allowing too many interlopers if it is chosen too large. Our dynamical analysis is most sensitive to this last criterion. We justify it a posteriori by noting below that our sample contains very few satellites with $300 < |\Delta v| < 500$ km s^{-1} even at small separations.

We estimate all distances from the recession velocity of the primary. Heliocentric velocities were corrected for Galactic rotation, assuming a rotational speed of 220 km s^{-1} for the local standard of rest, and for Virgocentric infall assuming an infall velocity $v_C = 300[\sin \delta_i \sin \delta_V + \cos \delta_i \cos \delta_V \cos (\alpha_i - \alpha_V)]$, where α_i and δ_i are the R.A. and decl. of the primary galaxy and α_V and δ_V are the R.A. and decl. of M87 (the center of the Virgo Cluster; Davis & Peebles 1983).

Our sample of satellites was compiled from two sources, a literature search, and a new spectroscopic survey to which we will refer to as the "fiber" survey. For the former we searched the *z*-cat and the HR catalog for galaxies satisfying our definition of a satellite. This route yielded a total of 34 satellites. Many positions and all the radial velocities measured from H I data come from the HR catalog. H I velocities with quoted errors <20 km s^{-1} and those without a quoted error, but which differ from the average of all velocity measurements for that object by less than 60 km s^{-1}, were averaged using the inverse of their quoted uncertainties as weights. For values without quoted errors we adopted $\sigma = 30$ km s^{-1}. We also took values for H I velocity widths from the HR catalog, when available. For a subset of the galaxies we were able to compare the recessional velocities with independent measurements obtained by W. Tifft (private communication); the distribution of differences has a dispersion of less than 10 km s^{-1}, supporting our view that the uncertainties[9] in most of the H I velocities are <20 km s^{-1}.

The starting point for our fiber survey was a list of faint galaxies around each of the primaries. These were obtained from digitized scans of POSS or ESO/SERC survey plates by the Automated Plate Measuring (APM) machine in Cambridge, England and from visual scans using the two-axis Grant machine at KPNO. In fields scanned both visually and with the APM machine, coordinates agreed to well within 1″, but the accuracy of star-galaxy classification was better in the visual scans. We therefore checked the star/galaxy classification of the APM fields visually in all cases. A field of radius 20′ typically contains about 20 galaxies down to a magnitude of $m_B \simeq 18.9$ (Seldner et al. 1977), only slightly fainter than our nominal limit of 18.5. As we discussed in § 1, the results of Lorrimer et al. (1993) indicate that typically only one or two of these will be genuine satellites. For this reason multiaperture spectroscopy is essential for our project. Due to the limited field of view of the telescopes we used, our fiber sample typically extends only to $r_p \sim 250$ pc, whereas the literature survey covered $r_p < 500$ kpc. Thus projected separations beyond 250 kpc are more sparsely sampled than smaller separations. The fiber survey, which we now discuss in detail, has so far yielded a total of 35 satellites. These are listed in Table 1.

3. OBSERVATIONS

3.1. *MX Observations*

MX is a multiobject spectrometer used at the Steward Observatory 2.3 m telescope on Kitt Peak (Hill 1984). Optical fibers are attached to 32 mobile probes. Each has a 2″ and a 4″ fiber, arranged on separate slits, together with a dedicated sky fiber. We used the 2″ fibers. The probes can travel radially to the center of the 45″ diameter field and azimuthally to 12°.25 either side of the center position. A standard Boller & Chivens Spectrograph with a 300 lines mm^{-1} grating was used to produce spectra from 3800 to 6000 Å with a resolution of about 8 Å. the detector was a TI CCD with readout noise of about $9e^-$. The main spectral features used for redshift deter-

[9] There is the possibility of systematic errors in the H I velocities due to beam contamination from the primary or companion galaxy. We found only one case where this appeared to be a problem (NGC 772/NGC 770).

TABLE 1

SATELLITES IDENTIFIED IN FIBER SURVEY

Spectrometer	Emission-Line Objects[a]	Absorption-Line Objects[a]
MX	N1620b, N2424a, N2718a, N3043a, N3614a, N3646a, N3735b, N4162a, N5297a, N7290b	N772a, N3646a, N3735a, N5297a
ARGUS	N895a, N3464a, N4679a, N5324a, N5324b, I4351b, N6948a, N6943a, N7038a, A2125a, N7083a	N259a, N488a, I4351a, N6943b, N7038b, A2120a, A2125b, N7083b
AUTOFIB (AAT)	...	N1459a
FOCAP	...	A1416a, A1416b
AUTOFIB (WHT)	...	N3154a

[a] Some satellites have both prominent emission and absorption lines.

minations were the Ca H & K lines at ~4000 Å and the emission lines Hβ, and [O III] λλ4959, 5007. For each field, two 1 hr exposures were obtained. The spectra were rescaled for differences in fiber throughput by using a twilight sky exposure. A master sky spectrum was composed from all the sky fiber spectra and then subtracted from each object spectrum. Each exposure was reduced independently using IRAF.[10] Radial velocities were determined from cross-correlation analysis (cf. Simkin 1974; Tonry & Davis 1979). All the spectra were also inspected visually. Velocity errors were typically ~70 km s^{-1}, which are small enough to identify satellites, but too large for our dynamical analysis. Follow-up observations at the MMT were therefore required.

Because of the low surface brightness of some of the targets, the inefficiency of the spectrograph, the mismatch of the spectrograph-spectrometer system, and the blind operation of probe positioning, the survey is not complete to the expected depth, ~18.5. Probe positioning improved with time because new observing techniques were implemented. Nevertheless, the system never performed entirely up to expectations. Out of 21 fields observed after probe pointing problems were corrected, 11 had at least one satellite, giving a total of 12 confirmed satellites in these fields, which we estimate below to be roughly 50% complete to ~18.5 mag. Three additional satellites in these fields (N1620a, N2718b, and N7290a) were found from the literature search.

3.2. *ARGUS Observations*

ARGUS is a multiobject spectrometer at the prime focus of the 4 m telescope at Cerro Tololo Interamerican Observatory (Ingerson 1987, 1988). At the time of our observations it had 24 object fibers plus 24 sky fibers each of 1".8 aperture. Like MX, it is based on the probe system. We used the bench-mounted spectrograph with the red camera and a 527 lines mm^{-1} grating with 3.4 Å resolution and coverage of 1860 Å: the detector was a GEC CCD. The spectra were centered at about 5100 Å, which allows viewing of Hβ, [O III], and Mg I lines.

Besides being on a larger telescope, ARGUS has several advantages over MX. The observer can interactively check the probe positioning using imaging optics and a fiber bundle located in a periscope carried on a robot arm. The object acquisition rate is therefore high. For example, in the best conditions we could see about 90% of the target objects, which we estimate to be brighter than an integrated B magnitude 19.5 mag, through the periscope camera. For objects that could not be seen on the TV, we either applied no probe shift or, if a systematic shift had been necessary for many probes, a blind shift. Shifts comparable to the fiber size or greater were required for most targets. The field solution was known to be poor, but there had been no effort to correct it in software because a new corrector had been ordered and because the periscope was available. The second significant advantage of ARGUS is the bench-mounted spectrograph. The stability it provides allows one to spend less time on calibration and to remove cosmic rays by direct comparison of two consecutive 1 hr images. The wavelength drift on the detector during a night is of order 0.01 of a pixel, primarily due to the evaporation of liquid N_2 in the CCD Dewar, which causes flexure in the camera-Dewer assembly (N. Suntzeff, private communication).

The observing procedure consisted of two 1 or 1.5 hr exposures of each field. Standard star observations were taken at the beginning, middle, and end of each night through different fibers. Each set of two object exposures was then combined using the cosmic-ray filtering described. above. The spectra were traced using a lamp flat (continuum lamp observed through all the fibers) and the same trace was applied to the object exposures. The 24 sky spectra in each exposure were median combined into one high-S/N master sky spectrum. The master sky spectrum was scaled and subtracted from each individual object spectrum. The rms deviations around the sky line at 5577 Å were evaluated, and a new scaling and subtraction was done for each spectrum. This was continued until a minimum was found, typically in about five to eight iterations. Velocities were measured using cross-correlation techniques for absorption-line systems and Gaussian line fitting for emission-line systems. Nightly systematic velocity shifts were derived from observations of standard stars and were typically less than 10 km s^{-1}. This was also the size of our velocity errors for standard stars. We therefore estimate the errors in the satellites' radial velocities to be <20 km s^{-1}. This is borne out by a comparison with previously measured velocities for a few objects, either from the HR catalog or from our own MMT observations.

Representative satellite spectra obtained with ARGUS are shown in Figure 1. The top panel shows the spectrum of an emission line satellite (I4351b; $m_B = 17.8$) with moderate S/N. The intermediate panel shows the spectrum of a bright satellite (N7083b; $m_B = 14$) with the most prominent absorption lines marked. The bottom panel shows one of the lowest S/N spectra (A2120a; $m_B = 19.8$) for which we were able to measure a velocity using the cross-correlation technique.

Twenty-two fields were observed with ARGUS. In most of them we discovered at least one satellite, giving a total of 19

[10] IRAF is distributed by the National Optical Astronomy Observatories, which are operated by AURA, Inc., under contract to the NSF.

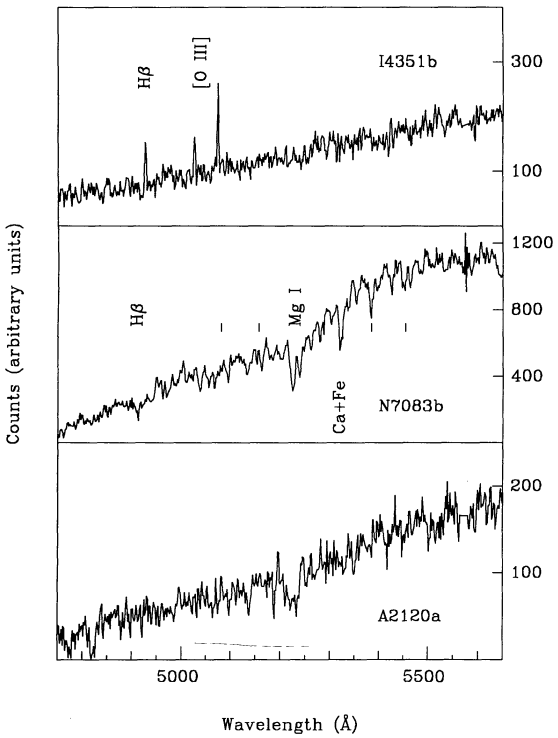

FIG. 1.—Spectra of three satellites discovered with ARGUS. The identification number of each object (see Table 3) is given in the upper or lower right-hand corner. Some of the brighter lines are identified and some fainter lines are marked (identifications from Sandage 1978).

satellites over all the fields. Four further satellites in these fields were found by our literature search (N259b, N488b, N5254a, and I4351c). From the analysis of Lorrimer et al. (1993), we conclude that the ARGUS survey is very nearly complete to ~18.5 mag. These numbers are discussed in more detail in § 4.

3.3. *AAT and WHT Observations*

All but a few hours of the 16 dark nights allocated over a period of 2 years to this project at the AAT and the WHT were lost to bad weather. In the few clear spells, we were able to identify four satellites (N1459a, N3154a, A1416a, A1416b). During our first run at the AAT we used the Automatic fiber Positioning System (AUTOFIB) which uses a robot arm to position 64 object fibers and six guide-star fiber bundles over the 40′ field of view. The fibers have a diameter of 2″, and the pointing is accurate to about 0″.1. Typically 50 fibers were assigned to program objects and 10 were used for sky determination. We used the RGO spectrograph with a 1200 lines mm^{-1} grating blazed in the blue providing a resolution of 1 Å $pixel^{-1}$. The spectral region between 3580 and 4600 Å was observed with the Image Photon Counting System (IPCS). For our second AAT run we switched to a plug-board system, the Fiber-Optic Coupled Aperture Plate (FOCAP), in order to use the wider 3″ fibers available; this is useful at a site where the seeing is often rather poor. FOCAP has 50 fibers, seven of which were dedicated to sky measurement. We used the same spectrograph and detector as in our first run, but with a 600 lines mm^{-1} grating, providing 2 Å $pixel^{-1}$ resolution between 3460 and 5495 Å.

For our WHT observations we used a pilot AUTOFIB system similar to that at the AAT. This system has 55 fibers, but the usable field of view at the telescope is only 17′. We used the FLEX spectrograph with a 632 lines mm^{-1} grating blazed at V, providing a wavelength coverage 2000 Å centered at 4480 Å and a resolution of 1.73 Å $pixel^{-1}$. The detector was a EEV CCD (1172 × 760 pixels).

The data for our AAT and WHT observations were reduced using FIGARO and the cross-correlation package of the Durham University Spectral Data Evaluation and Reduction System (DUSDERS). The procedures are similar to those described above for the ARGUS data. Velocity errors for absorption line determinations were estimated to be <30 km s^{-1} from fits to the correlation peak, calibrated previously with standard stars. The errors for emission-line determinations, estimated from Gaussian fits, are slightly smaller than this. Our first AAT run yielded the satellite of NGC 1459 (N1459a); our second AAT run those of A1416 (A1416a, b); and our WHT run that in NGC 3154 (N3154a; see Table 1).

3.4. *Follow-up Observations*

Follow-up observations were required to obtain velocities accurate to 20 km s^{-1} for satellites identified with the MX and also the satellites identified from *z*-cat. On the other hand, the H I measurements in the HR catalog were usually sufficiently accurate. The follow-up observations were carried out at the MMT, which was also used, together with the Steward Observatory 2.3 m telescope, to measure the rotation sense of some of the primaries.

At the MMT, we used the Red Channel spectrograph which has long-slit capability with high throughput and a CCD detector (for details see Schmidt, Weymann, & Foltz 1989). Object exposure times were limited to 15 minutes after which the flexure of the spectrograph can become important. The data were reduced in the standard manner. Typically 12–15 lines were identified in the calibration lamp exposures and a Chebyshev polynomial of order 4 or 5 was fitted to the lines. Sky subtraction was done along rectified columns with a low-order fit. We measured velocities from absorption lines using cross-correlation analysis and from emission lines using Gaussian line fitting. Heliocentric corrections were then applied.

In Figure 2 we compare our radial velocity measurements

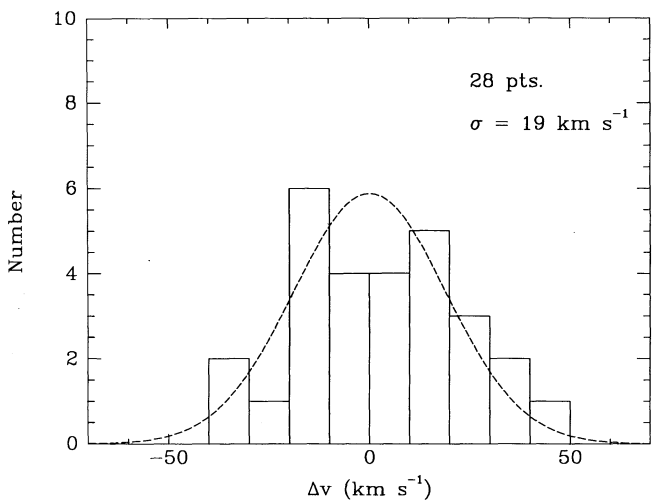

FIG. 2.—Histogram of the difference between radial velocities measured at the MMT and H I velocities from the Huchtmeier-Richter (1989) catalog for 28 galaxies. The dispersion, $\sigma = 19$ km s^{-1}, includes both the uncertainties in our measurements and those in the H I velocities.

with H I determinations from the HR catalog for 28 objects, most of which are primary galaxies. We do this by plotting the histogram of differences between the two determinations. The standard deviation of the distribution is slightly less than 20 km s^{-1}. Some of the galaxies have large-amplitude rotation curves, and the largest differences might be due to a slight misplacement of the slit. This problem should be negligible for satellite galaxies since they have smaller internal velocities.

We also measured the direction of rotation of many of the primary galaxies. At the MMT we used a 1200 lines mm^{-1} grating centered at 5100 Å, which gives a coverage of 650 Å and a resolution of 2.1 Å. At the Steward Observatory 2.3 m telescope, we used the Boller & Chivens spectrograph with a 1200 lines mm^{-1} grating. These observations are straightforward, and one can easily identify which side of the galaxy has the greater recessional velocity. The primaries are quite bright and short exposures, ~15 minutes, usually sufficed.

4. A SURVEY OF SATELLITES AROUND SPIRAL GALAXIES

In this section we present the data for our sample of satellites and discuss their main properties.

4.1. *The Data*

Our survey of satellite galaxies around bright spirals has so far yielded a total of 69 satellites around 45 primaries. Of these, 19 satellites were found with ARGUS, 12 with the MX (plus MMT folow-up), three with the AAT, and one with the WHT. The remaining 34 come from *z*-cat and the HR catalog. We did not observe 23 of the primaries in our list. In a further 17 we failed to detect any satellites, but this could be due, in part, to extraneous factors such as poor weather or inaccurate fiber positioning. The 40 primaries without known satellites are listed in Table 2.

Our survey is summarized in Table 3. The galaxies are listed in groups with the primary at the top, followed by its satellite(s). Column (1) gives the name of the primary or the identification number of the satellite. Columns (2) and (3) give right ascension and declination in 1950.0 coordinates. Column (4) gives the blue apparent magnitude, column (5), the heliocentric recession velocity, and column (6), the satellite/primary projected separation. This was calculated from the angular separation and the distance to the primary, estimated from the recession velocity and the corrections for LSR motion and Virgoncentric infall discussed in § 2.2. (Recall that we take $H_0 = 75$ km s^{-1} Mpc^{-1}.) Columns (7), (8), (9), and (10) give the galaxy type, the length of the major axis, the H I line width (uncorrected for inclination), and the inclination angle. The galaxy types are T-types as described in the Second Reference Catalogue of Galaxies (de Vaucouleurs, de Vaucouleurs, & Corwin 1976). Column (11) gives the position angle, i.e., the angle between a line connecting the nuclei of the primary and satellite, and the major axis of the primary. Finally, column (12) indicates the source of the radial velocity and whether the radial velocity was measured from absorption ("a") or emission ("e") lines and the source of the radial velocity ("A" indicates from the AAT, "C" from the CTIO 4 m, "H" from the HR catalog, "M" from the MMT, and "W" from the WHT).

The source of the magnitudes, coordinates, and types of our *z*-cat primaries and satellites is *z*-cat itself. The source of H I velocities, velocity widths, inclinations, types, and the coordinates of those galaxies with H I data is the HR catalog. The remaining coordinates come from the plate scans. The position angles and some magnitudes were measured visually from POSS and ESO/SERC plates. The uncertainty in the position angles, Θ_S^h, was estimated by comparing our values of major axis position angles with values in the literature. The 1 σ error in the position angle of the primaries is 5°, but the uncertainty in Θ_S^h is somewhat less than this because uncertainties in the direction to north cancel out.

Blue magnitudes were not available in the literature for many of our satellites. We estimated these by eye, using the Coma Cluster data of Godwin, Metcalf, & Peach (1983) as calibration. From a comparison with measurements in the literature, we estimate a 0.45 mag 1 σ error in our determinations. This large uncertainty reflects the lower surface brightness of our satellites compared to galaxies in the calibration field. For high surface brightness objects, our errors are considerably smaller. Whenever available, we preferred published data to our own low-precision magnitude measurements. Sizes and types were also estimated visually for many galaxies. Our estimated 1 σ uncertainty in the size is 0.5. To ensure homogeneity, all satellite sizes given in Table 3 are from our own measurements. Galaxy types are extremely uncertain, especially for galaxies of small angular extent, so the types listed in the table should be regarded only as approximate.

In Figure 3 we plot the histogram of magnitude differences between satellites and their respective primary. By definition, satellites must be at least 2.2 mag fainter than their parent galaxy, but, in fact, ~85% of the satellites have a magnitude difference greater than 2.5 mag. In Figure 4 we plot the difference, Δv, between the radial velocities of each satellite and its corresponding primary as a function of their projected separation on the sky, indicating satellites from our fiber and literature samples by circles and crosses respectively. In Figure 5 we plot the absolute value of this velocity difference, $|\Delta v|$, also as a function of projected separation. These plots depict our basic raw data, which we now discuss in detail.

4.2. *Interlopers*

By our definition, a satellite cannot have a velocity difference, $|\Delta v| > 500$ km s^{-1}, or a projected separation, $r_p > 500$

TABLE 2

PRIMARIES WITHOUT KNOWN SATELLITES[a]

NGC 803+	IC 1783	A0407−48*	IC 2070	NGC 2989	NGC 2990+
NGC 2701	NGC 2713	NGC 2870+	NGC 2939	NGC 3549+	NGC 5162
NGC 3200*	NGC 3320	NGC 3463	NGC 4793	NGC 4939+	NGC 5875+
NGC 3976	NGC 4602	NGC 4682	NGC 5633	NGC 5665	NGC 7309*
NGC 5172+	NGC 5362	NGC 5492+	NGC 6808	NGC 7124	NGC 7755
IC 5071*	NGC 6368+	NGC 6699*	NGC 7606*	NGC 7721*+	
NGC 7416*	NGC 7448	NGC 7541	NGC 2359	NGC 2608	

[a] These primaries satisfied the criteria described in § 2.1. Those that have been observed with ARGUS or MX are denoted with (*) or (+), respectively. This is not a complete sample.

TABLE 3

DATA FOR PRIMARY AND SATELLITE GALAXIES

Name (1)	α^a (2)	δ (3)	m_B (4)	$v_\odot^b$ (5)	r_p^c (6)	T^d (7)	a^e (8)	W_0^f (9)	i^g (10)	Θ_S^h (11)	S^i (12)
N259	0 45 30.0	−3 2 50	12.5	3808	...	4	3.2	456	81	...	Ma
N259a	0 44 44.6	−2 49 4	18.3	3518	249	9	0.5	...	...	2	Ca
N259b	0 46 20.6	−2 39 5	15.5	3996	375	10	0.5	...	...	67	Me
N488	1 19 10.9	4 59 36	11.6	2268	...	3	6.0	463	42	...	Ma
N488a	1 19 30.0	5 6 0	15.6	2212	64	−4	1.9	...	...	17	Ca
N488b	1 17 48.0	5 33 48	17.0	2170	322	10	1.6	108	50	44	H
N772	1 56 35.3	18 45 50	11.3	2468	...	3	8.0	480	51	...	Ma
N772a	1 56 28.2	18 42 46	14.2	2490	32	−4	1.0	...	42	76	Ma
N895	2 19 5.9	−5 45 0	11.5	2290	...	6	3.5	284	41	...	Ma
N895a	2 19 15.1	−5 45 47	17.3	2402	19	11	0.3	...	...	1	Ce
N1459	3 44 50.8	−25 40 24	13.6	4160	...	6	3.5	...	48	...	Ma
N1459a	3 44 52.4	−25 40 51	18.8	4009	9	10	2.0	...	...	27	A
N1620	4 34 3.7	−0 14 42	13.6	3513	...	5	3.2	452	69	...	Ma
N1620a	4 35 0.0	−0 24 0	16.5	3720	219	6	1.1	...	...	69	Ma
N1620b	4 34 58.3	−0 22 17	15.6	3670	203	−4	...	...	...	86	Me
N1961	5 36 33.9	69 21 16	12.2	3934	...	4	4.6	702	50	...	Ma
N1961a	5 38 54.0	69 16 0	15.4	3927	214	5	2.4	296	84	15	H
N1961b	5 37 6.0	69 13 0	15.6	3884	139	10	1.2	143	70	63	Me
N1961c	5 37 54.0	69 24 0	14.5	4122	120	3	1.0	186	55	30	Ma
N1961d	5 40 12.0	69 2 0	15.1	4305	435	10	1.1	151	...	40	Me
N1961e	5 39 24.0	69 8 0	15.0	4282	319	2	2.2	298	50	35	Me
N2424	7 37 16.4	39 20 58	13.9	3112	...	3	3.9	439	90	...	Ma
N2424a	7 37 42.1	39 16 55	18.5	2814	81	3	0.3	...	...	47	Me
N2718	8 56 11.5	6 29 17	13.3	3842	...	2	2.3	135	15	...	Ma
N2718a	8 56 41.6	6 31 25	17.0	3640	118	15	0.6	...	...	18	Me
N2718b	8 55 48.3	6 31 21	15.5	3551	93	15	1.1	...	...	22	Me
N2997	9 43 27.4	−30 57 35	11.0	1086	...	5	13.2	276	35	...	Ma
N2997a	9 41 55.0	−31 56 6	15.2	1209	251	10	2.4	70	...	56	H
N2997b	9 42 37.0	−31 35 42	13.2	1256	161	10	2.6	164	30	59	H
N2997c	9 43 18.0	−30 6 42	14.6	1004	207	7	4.9	148	79	78	H
N3043	9 52 41.3	59 32 40	13.3	2998	...	3	1.9	319	71	...	Ma
N3043a	9 53 51.0	59 13 46	16.6	3028	263	3	0.7	...	...	70	Me
N3154	10 10 18.1	17 16 42	14.5	6508	...	4	...	...	63	...	Ma
N3154a	10 10 15.2	17 16 42	16.3	6636	18	5	0.9	...	...	59	We
N3464	10 52 13.6	−20 47 55	13.2	3750	...	4	4.3	386	46	...	Ca
N3464a	10 51 24.0	−20 56 59	18.8	3807	217	10	0.2	...	...	77	Ce
N3614	11 15 35.2	46 1 16	12.7	2332	...	5	4.6	318	52	...	Ma
N3614a	11 15 40.1	45 56 11	18.5	2282	52	8	0.3	...	...	55	Me
N3629	11 17 51.9	27 14 13	12.9	1514	...	5	2.1	249	43	...	Ma
N3629a	11 21 46.5	27 43 54	16.0	1503	409	3	1.3	165	...	33	H
N3646	11 19 5.2	20 26 43	12.1	4250	...	5	3.8	540	55	...	Me
N3646a	11 19 36.6	20 29 0	14.7	4417	134	−2	1.7	...	...	25	Mea
N3735	11 33 4.8	70 48 42	12.4	2696	...	5	4.3	513	78	...	Ma
N3735a	11 30 12.1	70 40 2	15.3	2618	192	7	1.1	...	...	72	Ma
N3735b	11 31 6.7	70 52 13	17.6	2595	119	11	0.6	...	...	21	Me
N4030	11 57 50.3	−0 49 22	11.6	1460	...	4	4.2	354	41	...	Ma
N4030a	11 56 12.0	−1 10 30	14.6	1486	206	10	2.3	169	58	11	H
N4030b	11 58 18.0	−0 15 18	17.0	1939	414	10	1.9	72	39	31	H
N4030c	11 58 36.0	−1 1 6	14.4	1490	104	10	1.5	113	28	83	H
N4030d	12 1 47.0	−1 15 7	17.0	1465	410	10	1.4	130	33	76	H
N4162	12 9 19.4	24 24 5	12.6	2559	...	4	2.5	334	52	...	Ma
N4162a	12 9 2.3	24 18 25	16.5	2524	75	2	0.6	...	...	43	Me
N4679	12 44 46.0	−39 17 54	13.3	4647	...	4	4.4	436	61	...	Ha
N4679b	12 46 10.4	−39 17 9	16.5	4568	295	10	1.2	...	...	79	Ce
N4725	12 47 59.9	25 48 20	10.2	1207	...	2	12.0	419	43	...	Ma
N4725a	12 49 18.6	26 2 45	13.2	1190	132	10	4.0	215	64	12	H
N4725b	12 50 43.5	25 32 58	15.5	1140	230	11	0.7	...	...	75	Mea
N5073	13 16 42.0	−14 36 0	13.0	2736	...	5	3.5	416	90	...	Ma
N5073a	13 16 48.0	−14 52 0	15.5	2876	209	2	...	...	...	33	Me
N5085	13 17 33.5	−24 10 42	12.1	1957	...	5	5.0	245	42	...	Ma
N5085a	13 21 19.0	−24 24 12	17.8	2056	424	10	3.2	113	28	52	H
N5248	13 35 2.4	9 8 23	10.9	1153	...	5	6.8	285	45	...	Ma
N5248a	13 33 12.0	9 13 24	15.5	1164	150	10	3.4	150	83	24	H
N5254	13 36 58.5	−11 14 29	13.0	2311	...	5	2.6	354	57	...	Ma
N5254a	13 34 24.0	−11 35 0	15.8	2467	413	7	1.8	117	31	62	Ma
N5297	13 44 19.0	44 7 23	12.3	2406	...	4	5.8	451	80	...	Ma
N5297a	13 44 13.7	44 5 0	15.0	2266	27	−2	0.9	...	45	81	Mea
N5324	13 49 29.1	−5 48 42	12.6	3044	...	4	2.2	232	24	...	Ma
N5324a	13 49 31.9	−5 49 25	−9.9	3245	12	...	...	75	45	...	H
N5324b	13 48 46.7	−5 49 23	16.5	3036	133	3	0.7	...	...	57	Ce
I4351	13 55 2.0	−29 4 18	12.3	2664	...	4	11.8	...	81	...	Ha
I4351a	13 54 36.7	−29 9 18	18.8	2674	79	10	0.2	...	...	34	Ca
I4351b	13 54 36.2	−29 1 6	17.8	2650	69	10	1.9	...	...	74	Ce
I4351c	13 52 4.0	−28 53 30	17.8	2717	429	3	1.1	...	...	89	Me
A1416	14 16 29.6	−26 24 52	12.8	6809	...	...	4.8	...	48	...	Ma
A1416a	14 16 19.3	−26 35 57	15.3	6695	303	4	2.1	...	...	83	A
A1416b	14 16 18.4	−26 24 38	15.6	6855	67	11	0.7	...	...	16	A
N5768	14 49 2.3	−2 19 27	13.0	1959	...	5	2.0	206	32	...	Ma
N5768a	14 50 0.0	−3 21 0	15.2	1954	529	8	3.3	178	38	53	H
N5899	15 13 14.9	42 14 1	12.6	2576	...	5	2.8	551	76	...	Ma
N5899a	15 13 16.4	42 23 31	15.0	2562	106	3	2.1	457	71	20	Mea
N5965	15 32 50.1	56 51 8	13.4	3413	...	3	6.0	612	87	...	Ma
N5965a	15 32 58.0	57 28 4	15.6	3391	531	11	0.6	...	...	48	Me
N6181	16 30 9.4	19 55 48	12.5	2371	...	5	2.5	395	61	...	Ma
N6181a	16 29 12.8	20 17 30	14.7	2520	257	7	2.4	273	80	32	Me
N6384	17 29 59.0	7 5 43	11.5	1655	...	3	7.0	394	46	...	Ma
N6384a	17 25 41.9	7 27 40	15.0	1691	474	5	3.1	150	25	73	H
N6948	20 39 48.0	−53 32 18	13.2	3228	...	3	2.3	...	65	...	Ha
N6948a	20 39 12.6	−53 12 16	16.8	3637	243	8	1.0	...	...	49	Ce
N6943	20 39 48.0	−68 55 42	11.9	3142	...	5	...	437	63	...	Ha
N6943a	20 38 51.5	−68 45 13	16.6	3328	132	6	1.2	...	...	29	Ce
N6943b	20 42 36.4	−68 44 59	18.8	3092	210	−4	0.5	...	...	6	Ca
N7038	21 11 46.0	−47 26 56	12.4	4940	...	5	3.3	545	56	...	Ha
N7038a	21 13 40.0	−47 25 48	18.3	4965	354	−4	0.3	...	...	37	Ce
N7038b	21 13 2.3	−47 29 50	17.8	4985	242	−4	0.3	...	...	21	Ca
A2120	21 19 56.0	−45 59 6	12.6	2686	...	4	3.5	425	73	...	Ha
A2120a	21 19 55.5	−45 57 44	19.8	2825	13	10	0.2	...	...	62	Ca
A2125	21 25 9.0	−38 5 48	12.9	2567	...	5	4.1	...	60	...	Ha
A2125a	21 24 9.6	−38 4 20	16.0	2645	110	2	0.6	...	72	1	Ce
A2125b	21 25 29.6	−37 48 20	15.4	2708	167	8	0.9	...	...	3	Ca
N7083	21 31 48.0	−64 7 54	11.8	3113	...	5	3.8	410	53	...	Ha
N7083a	21 31 9.1	−64 24 36	18.3	3375	194	−6	0.2	...	...	3	Ce
N7083b	21 36 10.2	−64 8 8	14.0	3201	322	2	1.5	...	...	78	Ca
N7137	21 45 54.1	21 55 43	13.3	1691	...	5	1.6	187	30	...	Ma
N7137a	21 45 12.0	21 55 53	17.0	1833	66	9	1.3	123	66	...	H
N7177	21 58 18.5	17 29 50	12.2	1155	...	3	3.3	319	53	...	Ma
N7177a	21 56 42.0	17 56 0	15.1	1093	156	8	2.9	130	28	57	H
N7290	22 26 0.8	16 53 35	13.8	2900	...	5	1.7	271	53	...	Ma
N7290a	22 26 24.0	16 45 0	17.0	2947	114	10	1.5	...	...	3	Me
N7290b	22 27 19.8	16 35 35	17.9	2855	292	11	0.5	...	...	9	Me
N7678	23 25 58.2	22 8 50	12.7	3486	...	5	2.5	317	42	...	Ma
N7678a	23 26 14.9	21 57 0	15.4	3887	167	3	1.9	191	52	26	H
N7716	23 33 57.2	0 1 14	12.9	2570	...	3	2.3	239	35	...	Ma
N7716a	23 34 50.0	0 6 53	15.7	2678	136	8	3.5	143	51	32	H

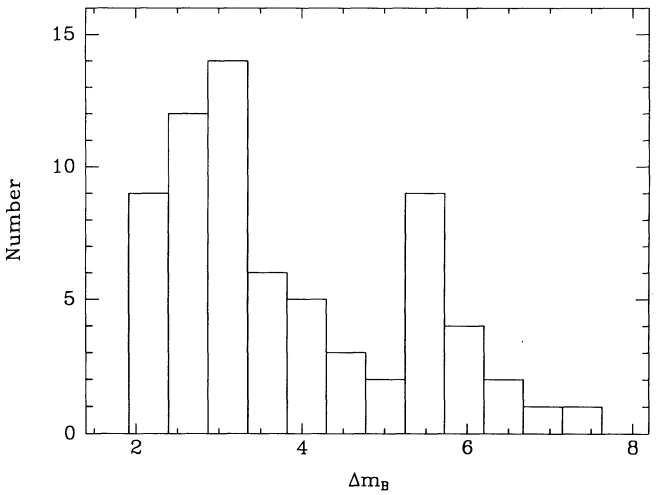

FIG. 3.—Histogram of the magnitude difference between satellites and their respective primary for the 69 satellites in our sample.

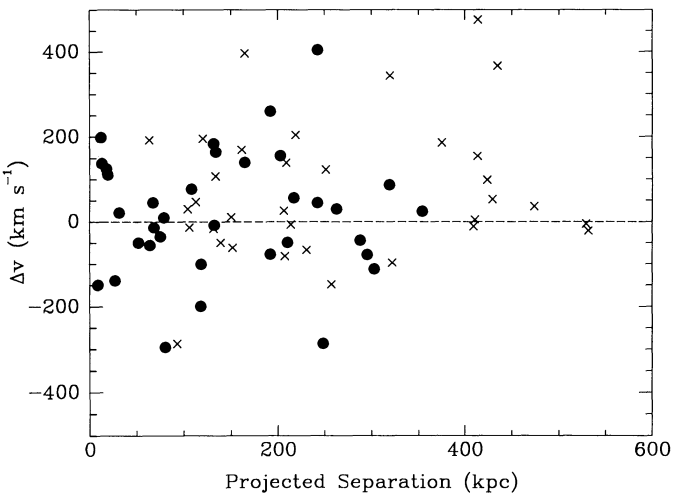

FIG. 4.—The difference, Δv, between the radial velocity of each satellite and that of its corresponding primary for the 69 satellites in our sample, as a function of their projected separation on the sky, r_p. The two satellites with $r_p > 500$ kpc had separations < 500 kpc before Virgocentric infall corrections were applied. Given the uncertainties in these distances, we decided to retain them in our sample. Crosses represent literature sample, and circles represent fiber sample.

kpc, relative to the primary. For most realistic mass models, these criteria will let in a few interlopers, faint galaxies whose distance from the primary is much greater in the radial direction than in the angular direction and are not part of the same physical system as the primary and its close satellites. Estimating the number or the identity of the interlopers is far from straightforward. A rough number may be obtained as follows. For the typical primary in the sample, we calculate the volume allowed by our satellite selection criteria. Assuming a uniform distribution of galaxies drawn from a Schechter luminosity function, we calculate the total number of galaxies in this volume that are faint enough to be classed as satellites but bright enough to be in our sample. We find a mean of about 1/20 of such "background" galaxies per primary, which we associate with interlopers.

Naively, we might expect our best guess for the number of interlopers to be 1/20 of the number of primaries. However, there is a further effect that needs to be taken into account. Nearly half of our satellites were found by searching existing redshift catalogs. There will be galaxies in these catalogs that satisfy our criteria for primaries but that do not have any satellites and are therefore not included in our sample. These

NOTES TO TABLE 3

[a] R.A. and Decl. are for 1950 epoch.

[b] Heliocentric velocity in km s^{-1}. Source of velocities given for MX (+MMT), ARGUS, AUTOFIB, and FOCAP observations in Table 1. The remaining velocities come from the HR catalog.

[c] Projected separation in kpc.

[d] Hubble type designated by T-types (cf. RC2).

[e] Major axis in arcminutes.

[f] H I line width in km s^{-1}, not corrected for galaxy inclination.

[g] Inclination in degrees. 0° indicates face on.

[h] Position angle in degrees. Described in text.

[i] Source of velocity (M = MMT, C = CTIO, A = AAT, W = WHT, and H = HR catalog). Spectral characteristics of spectrum (a = absorption, e = emission, ea = emission and absorption).

NOTES.—NGC 772a: H I measurements give a much lower velocity (2437 km s^{-1}); however, multiple optical measurements agree on the value presented in the table. The separation between primary and satellite is small, and the H I velocity determination of the satellite may have been affected by contaminating emission from the primary.

NGC 1459a: Probably an outer disk H II region.

NGC 1961: This galaxy is peculiar in several respects. First, it is among the most rapidly rotating disks known. Second, it has five companions, which is an abnormally large number of companions. Third, all five companions are located in the same quadrant with respect to the primary, suggesting that the companions belong to a group, possibly just seen in projection. We suggest later (§ 3.3.2) that at least two of the companions (13 and 14) are interlopers.

NGC 2424: The optical determination of the recessional velocity of the galaxy is significantly larger (3360 km s^{-1}) than the value quoted in the table from H I observations (Staveley-Smith & Davies 1987). The H I signal is convincing and samples the emission from the entire galaxy; however, further observations are necessary to resolve the discrepancy.

NGC 2718a, b: These two satellites appear to be interacting.

NGC 3646: Possibly an outlier of a relatively nearby cluster seen in projection.

NGC 5324a: There is an optical companion near NGC 5324 that could correspond to the observed H I emission. We have used the position used for fiber placement, but the true centroid of the companion is uncertain because it is projected onto the primary.

A1416: Has a relatively nearby cluster.

NGC 5899a: Anomolously large far-infrared flux ($L_{IR}/L_B > 14$). Bolometric magnitude for this satellite is greater than that of the primary. Should probably be rejected from sample.

NGC 5768: Only one H I velocity available for the galaxy (1959 km s^{-1} with unknown uncertainty); however, optical measurement from z-cat is 1951 km s^{-1}.

NGC 6384: Crowded environs. Although the primary satisfies the isolation criteria, there is a nearby concentration of galaxies.

NGC 7038: Crowded environs. Same as above.

NGC 7177: Uncertainty in primary velocity estimated to be greater than 20 km s^{-1} (25 km s^{-1}).

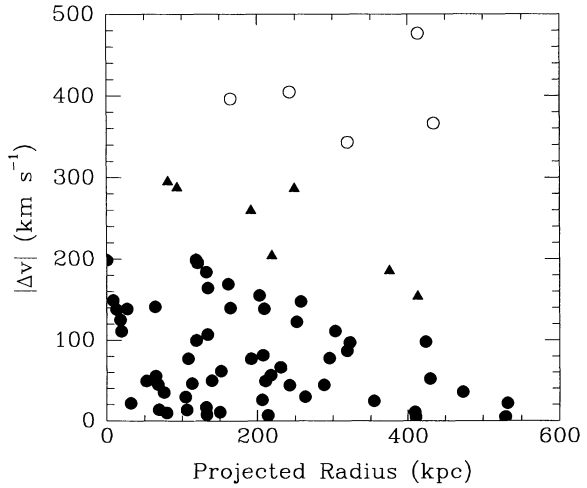

FIG. 5.—The absolute value, $|\Delta v|$, of the difference between the radial velocity of a satellite and that of its corresponding primary for the 69 satellites in our sample, as a function of their projected separation on the sky. Satellites coded by our opinion (see text) that they are interlopers.

are not all included in Table 2 because many were not targeted for fiber observations and so were not thoroughly examined (i.e., no visual inspection of POSS or ESO/SERC plates). Nevertheless, these should be counted when estimating the total number of primaries that we have effectively searched, especially if one considers the possibility that interlopers might be found more easily than genuine satellites. We estimate this number using z-cat. Here, there are 144 primaries with no satellites and 27 with at least one satellite, a ratio of 5.3.[11] In our final sample, 18 primaries with satellites came purely from existing redshift surveys, although not all from z-cat.[12] Thus, assuming the same ratio of 5.3 for this sample, we infer that we searched an effective number of 113 primaries. We would expect about 113/20 $\approx$ six interlopers around these primaries, although most of them are unlikely to appear in z-cat since the catalog seems to contain only about 20% of the true satellites (see below). Thus six is a conservative upper limit on the likely number of interlopers in the literature sample. The fiber sample contains 43 primaries which were not selected on the basis of having apparent companions. These might contribute 43/20 $\approx$ two interlopers. This number is also probably high because our fiber field rarely reached out as far as 500 kpc. Thus, we do not expect more than eight interlopers or 12% of our sample of 69 satellites. A more probable number is three or four.

Identifying and eliminating interlopers is even more difficult than estimating their number. A priori, one might expect them to be extreme objects, i.e., those with the largest $|\Delta v|$ or r_p. Zaritsky (1992) argues that a combination of small biases causes interlopers to have preferentially positive velocity differences. He argues that this explains the statistically significant excess of satellites with positive Δv which can be seen in Figure 4, and which is due almost entirely to the literature sample. Given the nature of small number statistics, only a small fraction of the excess must be accounted for to reduce the significance level of the observed asymmetry. However, if when the sample is enlarged the level of asymmetry remains constant, other explanations must be found. He also shows that interlopers are most likely found in systems with many apparent companions or in crowded environs. The level of contamination as determined from the statistics of the excess is consistent with that estimated above.

We have divided the background candidates into two groups based on their position in the $r_p - |\Delta v|$ plane (Fig. 5). The most likely interlopers are satellites N1961d, N1961e, N4030b, N6948a, and N7678a. Besides being the five objects with the largest $|\Delta v|$'s, they all have positive velocity differences, three belong to satellite groups of three or more members, and another lies in a field classified as crowded. Note that this set is already bigger than our best guess at the number of uncorrelated interlopers. The next most likely interlopers are satellites N259a, N259b, N1620a, N2424a, N2718b, N5254a, and N7083a. Unlike the first five objects, these do not have any particularly peculiar qualities. Furthermore, eliminating these would remove more than our upper limit on the number of interlopers in the sample. Thus our preferred sample, the one which we will use for most of the remainder of this paper, excludes *only* the first group of five objects. Evidently, excluding objects with large $|\Delta v|$'s from our dynamical analysis will reduce our estimate of primary mass. We therefore expect our final results to err conservatively toward small mass.

4.3. *Number of Satellites per Primary*

Estimating the number of satellites per primary is not easy because satellites were found using a variety of sources and techniques. The best data come from the ARGUS, AAT, and WHT surveys that are essentially complete to their magnitude limit in a known area of sky around each galaxy. The MX survey is worse because of incompleteness due to the observational difficulties discussed above. The catalog data are the worst because a variety of selection biases make it impossible to estimate the completeness level reliably.

The 4 m fiber surveys covered 25 primaries and found 23 satellites around 16 of these galaxies.[13] The literature search turned up a further four satellites beyond the fiber fields, all but one of these belonged to a primary with identified companions. Thus, out to the separations probed by the fiber fields (the average limit between 250 and 300 kpc), there is an average of nearly one satellite per primary. The MX sample covered 21 fields and detected 12 satellites around eleven primaries. Three further satellites were found from the literature. Thus in the regions surveyed by MX we found an average of only 12/21 = 0.6 satellites per primary, suggesting a completeness of only 62% relative to the 4 m surveys. This drop reflects the lower sensitivity of the telescope and the pointing problems we experienced. We argued above that our literature survey found one satellite for each 6.3 primaries. This is a success rate of only 16%, even though the search went out to 500 kpc in all cases, about twice the average cut-off radius for the fiber surveys. This number is so small because of the ill-defined selection criteria of z-cat and its low completeness level. From the 4 m

[11] This is a conservative estimate since it is more likely that satellites are found around galaxies in regions with the most extensive redshift surveys; primaries with satellites are therefore likely to be a biased subset of the z-cat galaxies.

[12] Recall also that when selecting primaries we examined the fields visually on POSS or ESO/SERC plates for nearby companions and searched through additional redshift and magnitude catalogs.

[13] Because of poor weather, we do not know how many of the primaries observed at the AAT and WHT truly have no satellites. This has a slight effect (slight because only four of the satellites come from these observations) on the discussion presented in this section.

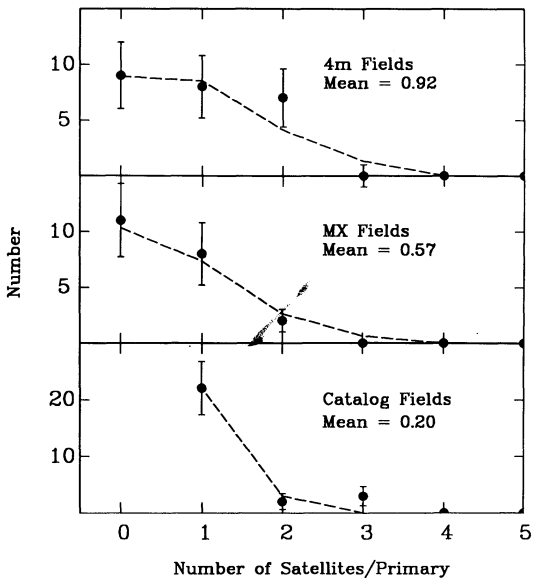

FIG. 6.—The distribution of satellites per primary in our various surveys. Circles denote the actual count and dashed lines represent a Poisson distribution with the means shown. Error bars are 1 σ assuming Poissonian statistics.

fiber surveys alone, we conclude that Sb/Sc spiral galaxies average about one satellite brighter than -15 (the magnitude limit is uncertain since the absolute magnitude limit obtained is different between fields) to projected radii between 200 and 300 kpc. This number is in excellent agreement with the results obtained by Lorrimer et al. (1993) from a cross-correlation analysis of the distribution of faint objects around a large sample of bright galaxies.

In Figure 6 we show the distributions of the number of satellites per primary (after exclusion of our five "interlopers") and compare them with Poisson distributions. Both the 4 m and the MX data are well represented by Poisson distributions. We conclude that the distribution of satellites is consistent with Poisson statistics. To our magnitude limit, multiple satellite systems are thus expected to be very rare. For example, with a Poisson mean of 1.0 the probability that a primary has five or more members is less than 0.004. The only such case in our sample is NGC 1961, and we argued above that two of its five satellites are interlopers. The statistical implausibility of so many satellites gives further weak justification for excluding these two objects.

Holmberg (1969) investigated the possibility that the number of satellites might be correlated with the luminosity of the primary. Unfortunately, his analysis had a large uncertainty since he had no velocity data and probed only out to 50 kpc. He found no significant correlation. However, even in the absence of a real effect, we might expect a correlation of this sort in our sample because our definition of satellite allows a brighter primary to draw companions from further up the luminosity function. We tested our sample for a correlation between the H I line width of the primaries and the number of satellites.[14] To do this, we split our sample at the median value of the H I line width and compare the distribution of the number of satellites per primary for the two resulting subsamples. A Student's t-test rules out the hypothesis that they have the same mean with only 84% confidence, so we conclude that there is no significant evidence that brighter galaxies have more satellites. This is a rather surprising result, confirming Holmberg's earlier work. The bias introduced by our satellite selection strategy does not appear to be strong.

4.4. *The Radial and Azimuthal Distribution of Satellites*

The surface density of satellites in our sample is plotted in Figure 7 as a function of projected separation from the primary. At small separations it follows a power law, but there is an abrupt change in slope beyond $r_p \simeq 300$ kpc; we attribute this break to lack of coverage at large radii in our fiber survey. (Recall that only our literature survey extended to $r_p = 500$ kpc.) The best-fit power law within $r_p = 300$ kpc has index of -1.0 ± 0.2, implying a *three-dimensional* number density profile, $\rho \propto r^{-2.0 \pm 0.2}$. This result is in reasonable agreement with the clustering studies of Lake & Tremaine (1980) and Lorrimer et al. (1993); the latter find a slope between -0.5 and -1.0 for the cross-correlation of faint with bright galaxies.

We have also investigated the azimuthal distribution of satellites with respect to the disk major axis in an attempt to search for the Holmberg effect: a statistical excess of objects along the minor axis out to a projected radius of 50 kpc. We measured the position angles of all the primaries and satellites in our sample from their images in POSS and ESO/SERC survey prints (see Table 3). In Figure 8 we plot the angle between the position of the satellite and the major axis of the primary as a function of projected separation. Only primaries with inclinations greater than 45° are considered in order to have accurate measurements of the major axis position angle. (Primaries with inclinations less than 50°, but still greater than 45°, are shown as solid squares.) The Holmberg effect is indeed just visible in our data: there is an apparent lack of objects at smaller angles for $r_p < 50$ kpc. However, the total number of objects with $r_p < 50$ kpc is so small that a KS test cannot rule out an underlying uniform distribution at more than the 2 σ level. Beyond $r_p = 100$ kpc, the distribution of angles appears uniform, although again with very small number statistics

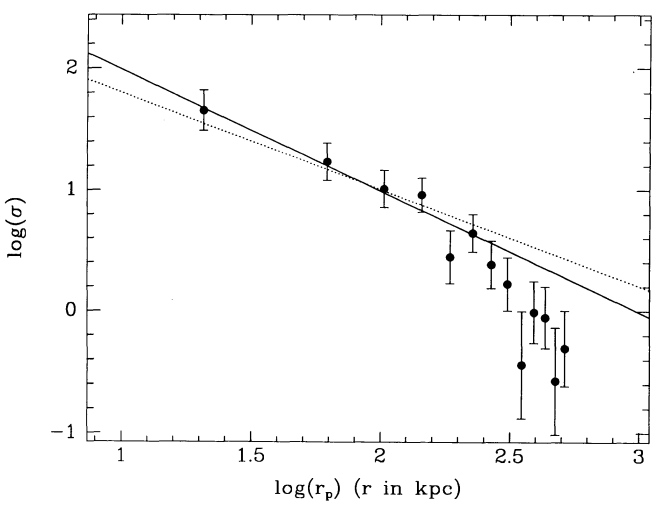

FIG. 7.—Number surface density against projected separation for the 69 satellites in our sample. The dotted line has slope -0.8 corresponding to a *three-dimensional* density run, $\rho \propto r^{-1.8}$. The solid line represents the best-fit line (slope $= -1.0$).

[14] There are six primaries for which we were unable to find 21 cm data. For these we derived a 21 cm line width from the magnitude and the Tully-Fisher relation.

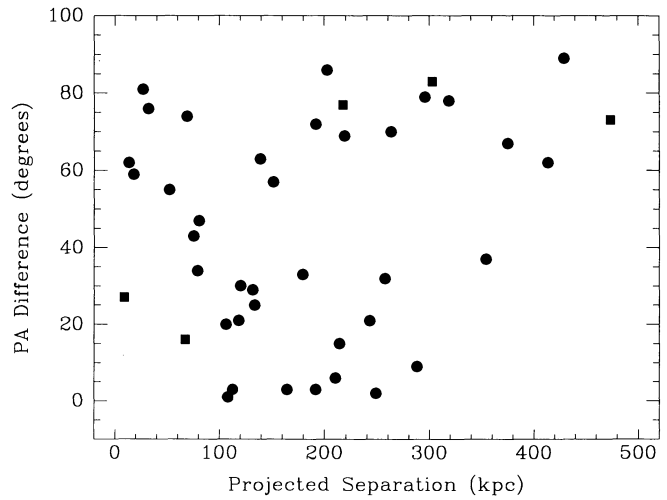

FIG. 8.—The difference between the position angle of the primary's major axis and the position angle of the satellites as a function of projected separation. Filled circles correspond to primaries with inclinations greater than 50° and solid squares to primaries with inclinations greater than 45° but less than 50°.

there is a lack of satellites with small position angle differences beyond 300 kpc. We conclude that there is no Holmberg effect beyond 50 kpc, but that our sample is too small for a definitive conclusion at smaller separations.

4.5. *Internal Properties of the Satellites*

In this section we consider the morphological, spectroscopic and photometric properties of the satellites. We begin by considering Hubble types that we express numerically through the system devised by de Vaucouleurs et al. (1976; see Table 3). In this system, larger numbers denote later types. In Figure 9, we plot the types of our satellites against their projected separation from the primary. There appears to be a weak tendency for type to increase with projected separation, an effect previously noted by Einasto et al. (1974). However, when we bin the data into early (−6 to 3) and late (7 to 11) types, we find mean projected separations of 187 kpc and 218 kpc, respectively. This difference is not significant according to a Student t-test. Using a KS test, we find no significant difference between the r_p distributions. We have also divided the sample at $T = 0$ and find, using a KS test, no significant difference between the two distributions. We conclude, therefore, that our data provide no significant support for the effect claimed by Einasto et al.

We also classified the 43 satellites for which we have spectra according to their spectral characteristics. The presence of emission or absorption lines is a crude indication of the age and star formation activity of the system. In Figure 10 we plot the distribution of projected separations for satellites whose spectra are dominated either by absorption or by emission lines, or have prominent lines of both kinds. There is an apparent excess of emission line objects, at *small* projected separations, perhaps reflecting interaction-induced star formation, but once again this trend is not significant in our (admittedly small) subsample. Note that, if real, the effect would be in the opposite sense to that suggested by Einasto et al.

The luminosity function of our satellites is shown in Figure 11. It is clearly well fit by a curve of Schechter form with $\alpha = -1.07$ and $L_* = 2.06 \times 10^{10}\ L_\odot$. The curve is arbitrarily normalized in the figure. Note that our magnitude measurements have large errors. Furthermore, our luminosity function is poorly determined because of incompleteness, because of selection effects induced by our definition of "satellite," and because of the different selection procedures in our "literature" and "fiber" samples. We have not attempted to correct for any of these effects. Note that most of the satellites are fainter than the LMC.

Visual inspection of our satellites on the POSS makes it clear that they can be separated into "normal" and "low surface brightness" objects. The latter tend to be galaxies whose major axis is larger than about 1′. This category is comprised of the satellites N488b, N1620a, N4030d, N5085a, N5254a, I4351a, I4351b, I4531c, N5768a, N6384a, N7177a, N7290a, and N7716a. Although our classification is fairly arbitrary, we can only stress that the difference is fairly obvious on

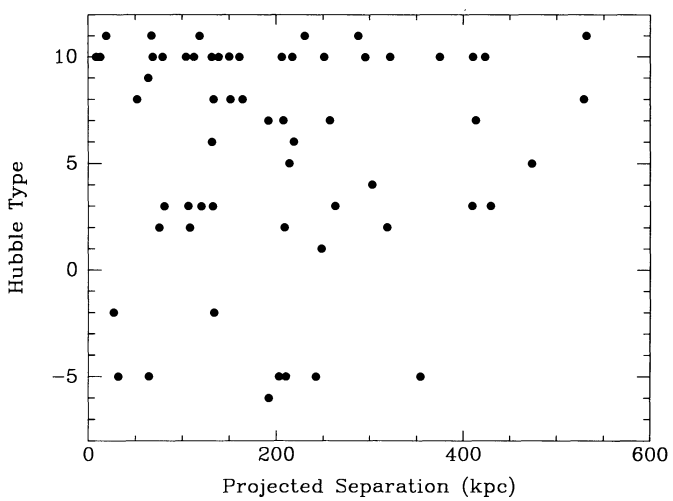

FIG. 9.—The Hubble type of the satellites (in the de Vaucouleurs et al. 1976 system) as a function of projected separation. Larger numbers correspond to later types.

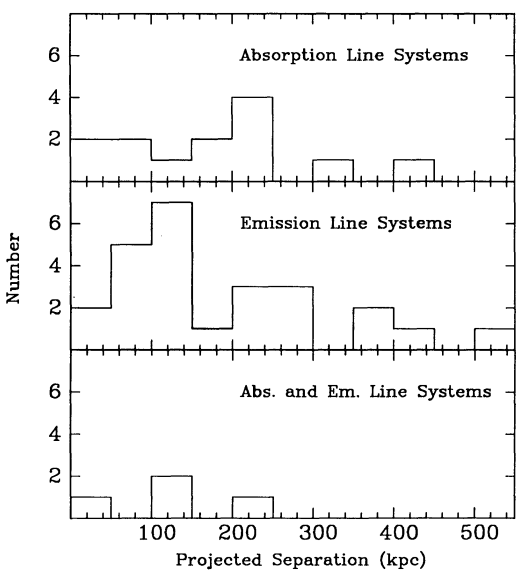

FIG. 10.—Histograms of projected separations for satellites with difference spectral characteristics.

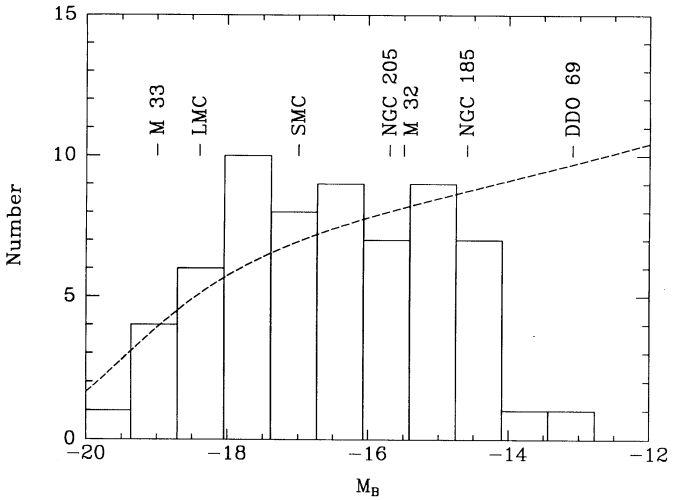

FIG. 11.—The luminosity distribution of satellites in our sample. Blue absolute magnitudes for Local Group members are indicated for comparison. Also plotted is a curve of Schechter's form with the parameters given in the text.

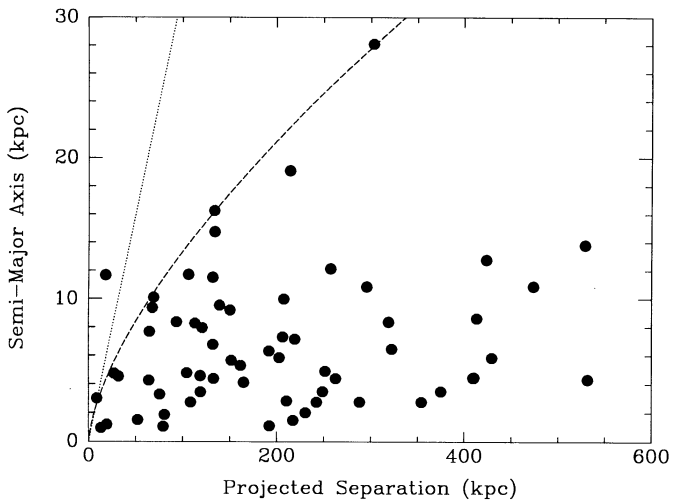

FIG. 13.—The semimajor axis of the satellites as a function of projected separation. The lines show the expected tidal radii assuming circular orbits and two different mass models for the primaries: a point mass model (*dotted line*) and an isothermal mass distribution (*dashed line*). See text for details.

inspection. Since even the lowest surface brightness galaxies are visible on sky survey plates, they are not the extreme of the population discussed by Impey, Bothun, & Malin (1988) and Bothun et al. (1990). In Figure 12 we plot histograms of projected separation for our two classes. The low surface brightness galaxies appear to lie at larger projected separations than the normal population. Indeed, a KS test rules out the hypothesis that the samples are drawn from the same parent population with 98.8% confidence (2.5 σ).

Previous studies of satellites, including globular clusters, have explored the possibility that their sizes may be tidally limited (e.g., Hodge 1966; Innanen, Harris, & Webbink 1983; Faber & Lin 1983). In Figure 13 we plot the semimajor axis of the satellites in our sample against projected separation from the primary. The rank correlation coefficient is 0.21, indicating a weak correlation significant at the 90% confidence level. The significance is increased to 96% (rank correlation coefficient 0.33) if we consider only those satellites with projected separation less than 200 kpc. Considering that any intrinsic correlation would be weakened by projection effects, we regard this result as clear evidence for a physical effect in our sample, at least out to projected separations of 200 kpc. A similar effect, out to somewhat smaller radii, is seen in the globular clusters of our own Galaxy (van den Bergh, Morbey, & Pazder 1991) and of M31 (Cohen & Freeman 1991).

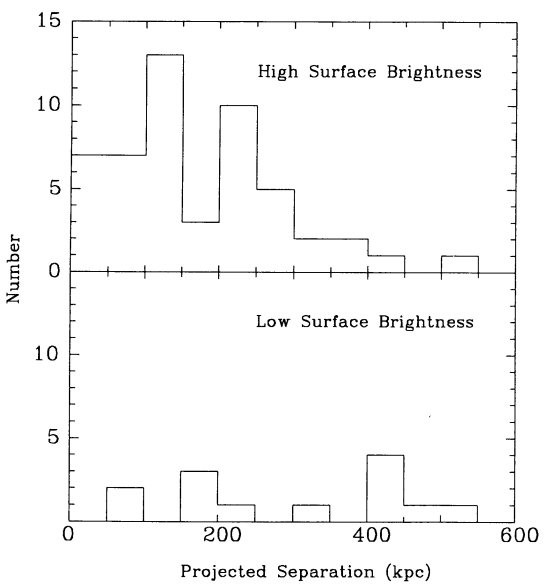

FIG. 12.—Histograms of projected separation for satellites with high and low surface brightness.

Several of the studies mentioned above have attempted to infer the mass of the parent galaxy from the hypothesis that globular clusters are tidally limited. This argument, however, has always been controversial because the result depends sensitiviely on the details of the tidal stripping mechanism and on the assumed cluster orbits. For what it is worth, we plot in Figure 13 the expected value of the tidal radius as a function of separation, assuming circular orbits and two galactic mass models (cf. Binney & Tremaine 1987). The dotted line corresponds to a point mass model and a ratio of satellite to primary mass of 0.1. For smaller ratios the line moves downward. The dashed line corresponds to an isothermal mass distribution with circular velocity, $V_c = 250$ km s^{-1}—the average for our sample—and satellite masses of $1 \times 10^{11}\ M_\odot$, which is about 10% of the inferred mass of the primaries (see below). In both cases only one satellite has a measured radius larger than the predicted tidal radius. It is clear, however, that tides in the point mass model are too weak to affect the observed radii of satellites unless their orbits are highly eccentric. The isothermal model, on the other hand, is quite consistent with tides determining these radii, even for near-circular orbits. We compared rough estimates of the satellite density to the density of the enclosed halo: L_{sat}/(semimajor axis)^3 versus V_c^2/r_p^2, where L_{sat} is the luminosity of the satellite and V_C is the circular velocity of the primary. Both of these quantities are extremely uncertain estimates of the relative densities, yet there is a significant correlation (probability of such a correlation arising at random is 0.012) between the two quantities, which suggests that tidal influences have played some part in determining the

TABLE 4

PROGRADE AND RETROGRADE SATELLITES

Sample	Satellites
Prograde	N259b, N772a, N1620a, N1620b, N1961c, N2424a, N3043a, N3646a, N4162a, N5073a, N5254a, N5297a, N5899a, N6181a, N6384a, N7083a, N7177a
Retrograde	N259a, N1961a, N1961b, N3154a, N3464a, N3614a, N3735a, N3735b, I4351a, I4351b, I4351c, N5965a, N7038a, N7038b, A2120a, N7083b, N7290a, N7290b

size of satellites. In the next section, we discuss a more direct method to estimate the mass distribution of the primaries.

4.6. *The Kinematics and Dynamics of the Satellite System*

In this section we investigate the limited kinematic information that can be extracted from our data and discuss simple estimates of primary mass. A more comprehensive discussion is deferred to a later paper.

For primaries that are nearly edge-on, we can easily distinguish between satellites that are on prograde orbits and satellites that are on retrograde orbits relative to the disk. The objects in each group are listed in Table 4. In Figure 14 we plot the velocity difference, Δv, against the signed projected separation, r_p, taken to be positive on the receding side of the primary, and negative on the approaching side. Thus, as indicated in the figure, prograde orbits correspond to quadrants I and III, while retrograde orbits correspond to quadrants II and IV. We also distinguish between satellites brighter (*open circles*), and fainter (*crosses*) than the median satellite luminosity, $M_B = -16.6$. There are several noteworthy features in this plot. First, the projected separation distributions are similar for the two kinds of orbit. (We have also checked that the distributions of position angle are similar and that neither group lies preferentially near the plane of the disk.) Second, there are almost equal numbers of prograde and retrograde orbits. Third, whereas retrograde satellites tend to have small values of $|\Delta v|$, prograde satellites, particularly those in quadrant I, tend to have large values. Finally, the satellites with large Δv's in quadrant I tend to be brighter than average.

The mean offset in the values of $|\Delta v|$ for prograde and retrograde orbits is most readily interpreted as the result of systemic rotation. Indeed, the mean rotation speed derived from the data in Figure 14 is $v_{\rm rot} = 29 \pm 21$ km s^{-1}. This value is sufficiently small that we need not be surprised that the numbers of prograde and retrograde orbits are so similar. Indeed, in Figure 15 we plot the histogram of signed velocity differences (prograde positive, retrograde negative) corrected for the inclination of the primary. The solid curve is a Gaussian centered at $v_{\rm rot}$ with dispersion $22 \times (35)^{1/2} = 124$ km s^{-1}. According to the Lilliefors test for normality (a statistic of the KS type applicable when parameters are estimated from the data; cf. Conover 1980), the model can be rejected only at the 88% confidence level. We therefore conclude that the distribution of Δv is consistent with a small amount of rotation in the satellite system, ~ 30 km s^{-1}, in the same sense as the disk. The correlation between orbital direction and satellite luminosity remains a puzzle. The difference in the distributions of absolute magnitude for the prograde and retrograde satellites is significant at the 95.5% confidence level. The sample, however, is rather small, and we prefer to wait for further data before hazarding a detailed interpretation of this point.

Another puzzling feature of our data is revealed by Figure 16, a scatter plot of the satellite/primary velocity difference, $|\Delta v|$, against primary circular velocity. We take the latter to be $V_c = W_i/2$, where W_i is the neutral hydrogen line width corrected for inclination. For primaries without H I data, we derived a line width from the blue absolute magnitude by assuming a "Tully-Fisher relation" of slope -10 (a value between the extremes of -5.03 [Bottinelli et al. 1983] and -13 [Rubin, et al. 1980]) normalized from the remaining primaries. Suspected interlopers are shown as open circles. There is no strong correlation between $|\Delta v|$ and V_c, a rather surprising result given the tight relationship between characteristic velocity and luminosity in the inner regions of spirals. This situation is reminiscent of binary galaxies (White et al. 1983; Charlton &

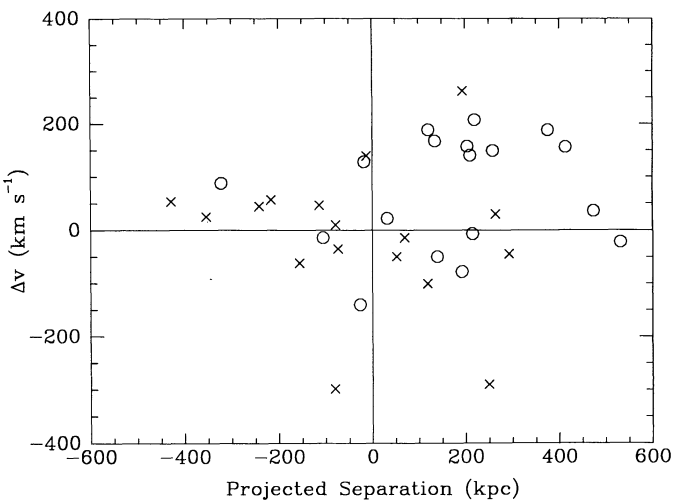

FIG. 14.—Velocity difference as a function of the signed projected separation. Prograde satellites with positive Δv and retrograde satellites with negative Δv are assigned positive r_p. Prograde satellites with negative Δv and retrograde satellites with positive Δv are assigned negative r_p. Satellites brighter or fainter than $M_B = -16.6$ (the median value for the sample), are indicated by open circles and crosses respectively.

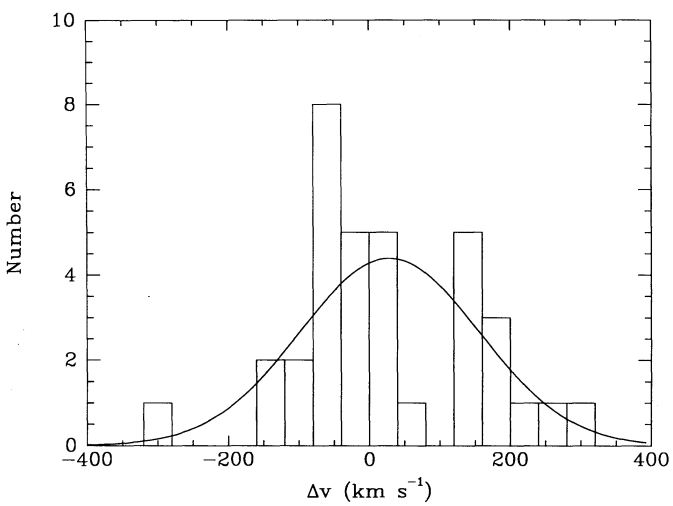

FIG. 15.—Histogram of signed velocity differences. Prograde or retrograde orbits are assigned positive or negative velocity differences respectively. The solid line is a Gaussian with mean and standard deviation derived from the data. A Lilliefors test shows that this model is rejected by the data at no more than the 88% confidence level.

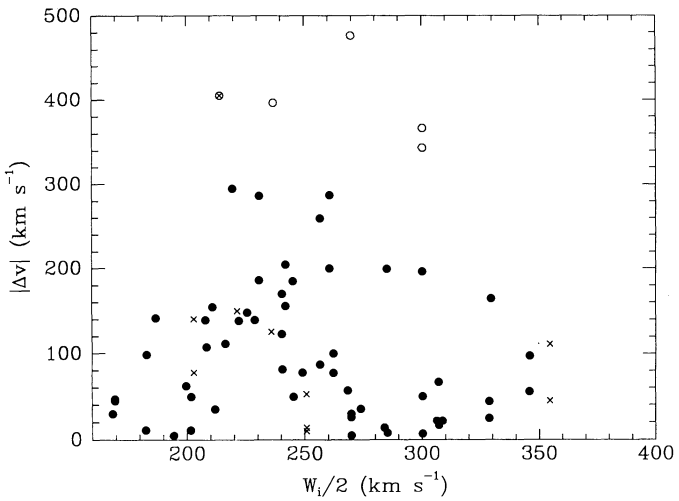

FIG. 16.—The absolute value of satellite/primary velocity difference as a function of the circular velocity of the primary. Satellites without H I data (for which V_c was derived from the Tully-Fisher relation) are indicated by crosses. Probable interlopers are shown as open circles.

Salpeter 1991). It may be due in part to contamination by projection effects and observational errors or it may be telling us something rather fundamental about galaxy formation. Detailed modeling is required to address this issue, and we defer this to a later paper.

Despite the puzzle presented by Figure 16, we can proceed to derive a rough estimate of the mean mass of our primaries. We take the characteristic velocity difference of a given sample of satellites to be the median value for this sample. In the presence of interlopers, this is a more robust quantity than the dispersion, which is sensitive to outlying values. We split the satellite sample into three radial bins with about equal numbers of objects. These have median $|\Delta v|$'s of 101, 80, and 98 km s^{-1} for bins with radii between 0 and 119, 120 and 242, and 243 and 531 kpc, respectively. If we remove the five likely interlopers (see § 4.2), the median values are 78, 101, and 67 km s^{-1} this time for bin boundaries between 0 and 114, 118 and 219, and 230 and 531 kpc respectively. Note that the characteristic velocity remains approximately constant with radius.

The minimum mass a primary can have if an observed satellite is to be bound is $M_{\rm min} = r_p \Delta v^2/2G$. The medium values of this minimum mass for the three radial bins of the last paragraph are $M_{\rm min}^{\rm med} = 2.4 \times 10^{10}$, 1.4×10^{11}, and $1.4 \times 10^{11}\ M_\odot$, respectively. These values are expected to be severe underestimates of the true mass because the true separation and the true relative velocity will exceed r_p and $|\Delta v|$, often by a large factor, because the actual satellite orbits will be subparabolic, and because significant mass may lie outside the position of many of the satellites. Models for binary galaxies indicate that the median minimum mass may be a factor (10–30) times smaller than the true mass, depending on the nature of the satellite orbits (White 1981).

A more realistic estimate of primary mass can be obtained by assuming that the mass distribution of the dark halos can be approximated as an isothermal sphere and that the velocity differences have an isotropic and Gaussian distribution. We then estimate the mass contained within radius r as $M = 2f^2 r[(\Delta v)_{\rm med}]^2/G$ where $f = 1.48$ is the ratio of the rms value to the median value of a half-Gaussian. For satellites within 50, 100, 150, and 200 kpc we find $(\Delta v)_{\rm med} = 139$, 120, 100, and 105 km s^{-1}, respectively, corresponding to $M = 6.3 \times 10^{11}$, 1.5×10^{12}, 1.5×10^{12}, and $2.2 \times 10^{12}\ M_\odot$. (This method cannot be applied at larger separations where the satellite population may not yet be in dynamical equilibrium.) Even this rough analysis gives a clear-cut indication that late-type isolated spirals are embedded in very extended massive halos.

5. DISCUSSION AND CONCLUSIONS

We have presented data from a large survey of faint satellites of spirals. Our primary motivation for undertaking this survey was to measure the mass of galaxies similar to the Milky Way and to test the possibility, put forward by Little & Tremaine (1987) among others, that their dark halos might be truncated at a few tens of kiloparsecs from the center. If correct, this view would have far-reaching implications for theories of galaxy formation: truncated halos would be very difficult to reconcile with formation through hierarchical gravitational clustering in a flat universe. In theories of this kind, galaxies form within dark matter clumps that typically extend out to their nearest neighbor; this may be clearly seen, for example, in the N-body simulations of Frenk et al. (1985, 1988) and Efstathiou et al. (1988b). Thus, the distribution of dark matter around galaxies provides one of the cleanest tests of a broad class of models which includes the standard cold dark matter cosmogony.

To carry out a dynamical analysis, it is essential to select a homogeneous sample of galaxies. Our approach is based on the premise that we can treat satellites of different galaxies as a statistical *ensemble*. Clearly, this is most easily interpreted if the potential wells of the parent galaxies are similar. We tried to ensure this by imposing strict selection criteria on the morphology and luminosity of our sample. We also required primaries to be relatively isolated to avoid disturbed mass distributions. Although the luminosity distribution of our primary sample is sharply peaked around $M_B = -20$, we also included galaxies within a relatively wide range of luminosities to test for systematic effects as a function of primary luminosity. Somewhat surprisingly, we were unable to detect any correlation between the luminosity of a primary and the orbital velocities of its satellites. This result suggests that the inner and outer regions of galaxy halos may not be well correlated even for isolated systems.

This paper presented the basic properties of our survey. From our own multifiber spectroscopy data and from a literature search, we have collected a total of 69 satellites with projected distance from the primary of less than 500 kpc. Most of the satellites are fainter than the LMC. Roughly $\frac{2}{3}$ have strong emission lines. There is on average about one satellite per primary in our survey, and the distribution of satellites per primary is Poissonian. The projected density profile of the *ensemble* of satellites falls off roughly as r_p^{-1}, implying a true radial number density profile that falls off as r^{-2}. The abundance and radial distribution of satellites are consistent with the results of an independent study of the projected galaxy distribution over a large region of sky (Lorrimer et al. 1993). At projected separations less than 50 kpc, the azimuthal distribution of our *ensemble* shows marginal evidence for the excess of satellites along the primary's minor axis originally noted by Holmberg (1969). There is no evidence for this effect at large separations.

Some of the satellites in our sample appear distinctly diffuse on sky survey plates. They tend to have large projected separations as one might expect if satellites are tidally truncated.

Although the correlation between size and separation is rather weak, it is in the sense expected from tidal effects and gives a first indication that the parent galaxies may have massive halos extending at least out to 200 kpc. To explore this further, a proper treatment of the kinematics and dynamics of the satellite population is required. Here we have presented only a simple, virial-type, calculation, but a more detailed study will appear in a forthcoming paper.

There is a marginal detection of systemic rotation in our sample of satellites. Satellites in prograde orbits tend to have larger velocity differences than satellites in retrograde orbits. From the 35 satellites whose primaries are nearly edge-on, we find a rotation velocity of 29 ± 21 km s^{-1} in the same sense as the disk. We find that prograde satellites are significantly brighter than retrograde satellites, but our sample is too small for us to be confident of this result. The characteristic velocity of the satellites relative to their primary remains approximately constant with radius out to the limit of our survey, ~ 250 kpc. Assuming an isotropic satellite velocity distribution within an isothermal dark halo, the implied circular velocity of a typical halo is ~ 200 km s^{-1}, implying a mass within 200 kpc of $2 \times 10^{12}\ M_{\odot}$. This is the main result of our survey: spiral galaxies similar to the Milky Way do indeed appear to have very massive extended dark halos.

This work was part of a Ph.D. thesis submitted to the University of Arizona. We would like to thank Scott Tremaine for encouragement when we started the project; J. Black, J. Charlton, and E. Olszewski for valuable input; and J. M. Hill for the use of the MX Spectrometer, which was funded by the NSF under grant AST-8116965, his assistance, and his cross-correlation software. We are grateful to M. Irwin for his efficient execution of APM scans, to S. Maddox for providing data from the APM Southern galaxy survey, and to KPNO for the use of their two-axis Grant machine. We also thank the support staffs of the MMT, Steward 2.3 m, CTIO telescopes, WHT, and AAT for their assistance. D. Z. acknowledges support from the NSF through a graduate fellowship and AST-8822297, and travel support from CTIO. Support for this work was also provided by NASA through grant HF-1027.01-91A from STScI, which is operated by AURA, Inc., under NASA contract NAS5-26555. C. S. F. acknowledges a Nuffield Foundation Science Research Fellowship.

REFERENCES

Begeman, K. 1987, Ph.D. thesis, Groningen
Binney, J., & Tremaine, S. 1987, Galactic Dynamics (Princeton: Princeton Univ. Press)
Bothun, G. D., Schombert, J. M., Impey, C. D., & Schneider, S. E. 1990, ApJ, 360, 427
Bottinelli, L., Gouguenheim, L., Paturel, G., & de Vaucouleurs, G. 1983, A&A, 118, 4
Charlton, J. C., & Salpeter, E. E. 1991, ApJ, 375, 517
Cohen, J. G., & Freeman, K. C. 1991, AJ, 101, 483
Conover, W. J. 1980, Practical Nonparametric Statistics (New York: John Wiley and Sons), 357
Davis, M., & Peebles, P. J. E. 1983, ARA&A, 21, 109
de Vaucouleurs, G., de Vaucouleurs, A., & Corwin, H. G., Jr. 1976, Second Reference Catalogue of Bright Galaxies (Austin: Univ. of Texas Press) (RC2)
Efstathiou, G., Ellis, R. S., & Peterson, B. A. 1988a, MNRAS, 232, 431
Efstathiou, G., Frenk, C. S., White, S. D. M., & Davis, M. 1988b, MNRAS, 235, 715
Einasto, J., & Lynden-Bell, D. 1982, MNRAS, 199, 67
Einasto, J., Saar, E., Kaasik, A., & Cherin, A. D. 1974, Nature, 252, 111
Erickson, K., Gottesman, S. T., & Hunter, J. H., Jr. 1987, Nature 325, 779
Faber, S. M., & Lin, D. N. C. 1983, ApJ, 266, L17
Freeman, K. 1970, ApJ, 160, 811
Frenk, C. S., White, S. D. M., Efstathiou, G., & Davis, M. 1985, Nature, 317, 595
Frenk, C. S., White, S. D. M., Davis, M., & Efstathiou, G. 1988, ApJ, 327, 507
Godwin, J. G., Metcalf, N., & Peach, J. V. 1983, MNRAS, 202, 113
Hill, J. M. 1984, Ph.D. thesis, Univ. of Arizona
Hodge, P. W. 1966, AJ, 66, 249
Holmberg, E. 1969, Ark. Astron., 5, 305
Huchra, J. P. 1987, The CfA Redshift Catalogue (z-cat)
Huchtmeier, W. K., & Richter, P.-G. 1989, H I Observations of Galaxies (New York: Springer-Verlag) (HR)
Impey, C., Bothun, G., & Malin, D. 1988, ApJ, 330, 634
Ingerson, T. E. 1987, in Instrumentation for Ground-based Optical Astronomy, ed. L. B. Robinson (New York: Springer-Verlag), 222
———. 1988, in Fiber Optics in Astronomy, ed. S. C. Barden (ASP Conf. Ser., 3), 99
Innanen, K. A., Harris, W. E., & Webbink, R. F. 1983, AJ, 88, 338
Lake, G., & Tremaine, S. 1980, ApJ, 238, L13
Little, B., & Tremaine, S. 1987, ApJ, 320, 493
Lorrimer, S. J., Frenk, C. S., Smith, R. M., White, S. D. M., & Zaritsky, D. 1993, in preparation
Moore, B., & Frenk, C. S. 1990, in Dynamics and Interactions of Galaxies, ed. R. Wielen (Heidelberg: Springer-Verlag), 410
Nolthenius, R., & White, S. D. M. 1987, MNRAS, 225, 505
Norris, J. E., & Hawkins, M. R. S. 1991, ApJ, 380, 104
Rubin, V. C., Burstein, D., & Thonnard, N. 1980, ApJ, 242, L149
Rubin, V. C., & Ford, W. K., Jr. 1970, ApJ, 159, 379
Rubin, V. C., Ford W. K., Jr., & Thonnard, N. 1978, ApJ, 225, L107
Sandage, A. 1978, AJ, 83, 904
Schmidt, G., Weymann, R. J., & Foltz, C. B. 1989, PASP, 101, 713
Schweizer, L. Y. 1987, ApJS, 64, 427
Seldner, M., Seibers, B., Groth, E. J., & Peebles, P. J. E. 1977, AJ, 82, 249
Simkin, S. M. 1974, A&A, 31, 129
Staveley-Smith, L., & Davies, R. D. 1987, MNRAS, 224, 935
Tonry, J., & Davis, M. 1979, AJ, 84, 1511
Tully, R. B., & Fisher, J. R. 1977, A&A, 54, 661
Vader, J. P., & Sandage, A. 1991, ApJ, 379, L1
van den Bergh, S. 1980, in NATO ASI, The Structure and Evolution of Normal Galaxies, ed. S. M. Fall & D. Lynden-Bell (Cambridge: Cambridge Univ. Press), 201
van den Bergh, S., Morbey, C., & Pazder, J. 1991, ApJ, 375, 594
White, S. D. M. 1981, MNRAS, 195, 1037
White, S. D. M., Huchra, J., Latham, D., & Davis, M. 1983, MNRAS, 203, 701
White, S. D. M., & Rees, M. J. 1978, MNRAS, 183, 341
White, S. D. M., & Zaritsky, D. 1992, ApJ, 394, 1
Zaritsky, D. 1991, Ph.D. thesis, Univ. Arizona
———. 1992, ApJ, 400, 74
Zaritsky, D., Olszewski, E. W., Schommer, R. A., Peterson, R., & Aaronson, M. 1989, ApJ, 345, 759
Zaritsky, D., & White, S. D. M. 1993, in preparation